Powder Technology 305 (2016) 98–107

Contents lists available at ScienceDirect

Powder Technology

journal homepage: www.elsevier.com/locate/powtec

An experimental investigation on hydrocyclone underflow pumping

Reza Sabbagh, Michael G. Lipsett, Charles R. Koch, David S. Nobes*

The Department of Mechanical Engineering, University of Alberta, Edmonton, AB T6G 2G8, Canada

ARTICLE INFO

Article history:
Received 30 December 2015
Received in revised form 12 July 2016
Accepted 22 September 2016
Available online 26 September 2016

JEL classification:
00-01
99-00

Keywords:
Hydrocyclone
Underflow pump
Pressure ratio
Model
Correlation
Control

ABSTRACT

The efficiency of a hydrocyclone is highly affected by the inlet flow conditions. Any fluctuation in the feed flow rate or feed solid concentration directly changes the separation performance. The underflow is typically adjusted to overcome the variable conditions of the feed flow, thereby delivering desired performance. A pump in the underflow allows active control of the hydrocyclone separation performance through either providing back pressure or by pump suction.

The effects of underflow pumping at different inlet conditions are investigated experimentally. The ratio of the absolute underflow pressure to the overflow pressure is defined as pressure ratio P^* and is used to compare the results. The pressure ratio resulting from underflow pumping has a similar effect in hydrocyclones as changing the underflow pipe size. For instance, increasing the pressure ratio (less pumping in the underflow) is similar to decreasing the underflow pipe diameter. The operating parameters of flow ratio R_f and inlet solid volume concentration c are found to have significant effect on pressure ratio. A nonlinear model for predicting pressure ratio is found to be $P^* = R_f^{-0.2689}\exp(-0.0267c)$ and has a maximum uncertainty of ±13% for the conditions tested. This prediction could be useful for controlling the underflow to maintain the desired hydrocyclone performance under varying inlet conditions.

1. Introduction

Hydrocyclones are used in industrial processes to separate liquid or solid particles from a bulk liquid phase of different density [1]. The mixture is usually pumped to the inlet pipe where it is directed tangentially to the hydrocyclone chamber. The flow starts to rotate and the centrifugal force due to rotation pushes the denser phase toward the hydrocyclone wall, increasing the concentration of the denser phase near the wall. The particles in the highly concentrated part of the flow leave the chamber through the outlet pipe. However, since separation is not always perfect, a portion of each phase leaves the hydrocyclone at both the overflow and underflow.

Hydrocyclones are considered to be relatively low capital cost devices that are easy to install. High capacity, simplicity, and low maintenance cost are further advantages of hydrocyclones [2]. However, separation performance of a hydrocyclone is affected by the inlet flow conditions, which is a major disadvantage when upstream flow conditions fluctuate [3]. In a solid-liquid hydrocyclone, changes in the inlet flow rate [4], particle size distribution [1,5,6], particle shape [7], and concentration [8] affect the outlet flow properties. Changes in the separation efficiency as a function of the separation cut size (the particle size that has 50% chance of being separated in the device) and the flow ratio R_f (the ratio of the volumetric underflow flow rate to the feed flow rate) are observed. For some operating conditions, this may even lead to impracticability of using a hydrocyclone. Controlling the hydrocyclone performance would allow a process to avoid such conditions [5].

There are several methods available for monitoring and controlling hydrocyclone performance. These methods are either based on the shape of the air core [9–12], the internal particle distribution [13], the shape (spray/rope) or other properties of the underflow [14,15]. The control typically actuates a flow stream at either the inlet [16] or the outlets [17,18]. A set of hydrocyclones that are used in a group have been controlled by regulating the overflow [3]. Some other methods to control the device separation performance include injecting water through the hydrocyclone wall [19], water injection to the underflow discharge pipe [20], and using an electrical hydrocyclone [21].

The flow stream in a hydrocyclone is usually controlled by changing the geometry, especially the apex size (shown in Fig. 1). Changing the apex size changes the underflow capacity and therefore the solids concentration and the separation cut size [22,23]. Commercial hydrocyclones are often supplied with several replaceable orifice sizes to allow the appropriate size to be used based on typical operating conditions. In addition, several designs for the underflow orifice are available [1,5]. Different types of discharge orifices that are used for manipulating the underflow are discussed in [5].

* Corresponding author at: Mechanical Engineering Department, University of Alberta, Edmonton, AB, Canada.
E-mail address: david.nobes@ualberta.ca (D. Nobes).

http://dx.doi.org/10.1016/j.powtec.2016.09.045
0032-5910/

Nomenclature

B	Bias (systematic) uncertainty
c	Volume fraction of solid particles in the inlet mixture
c_u	Underflow solid volume concentration (fraction)
D	Hydrocyclone diameter
d'_{50}	Reduced 50% separation cut size
D_i	Inlet pipe hydraulic diameter
D_o	Overflow pipe diameter
D_{50}	Median in particle size distribution
$G'(x)$	Reduced grade efficiency function
$G(x)$	Grade efficiency function
L	Hydrocyclone total length
l	Vortex finder length
L_1	Cylindrical section length
n_{FPS}	Feed pump speed
n_{UPS}	Underflow pump speed
P^*	Pressure ratio
P_i	Inlet pressure
P_o	Overflow pressure
P_u	Underflow pressure
P_x	Precision (random) uncertainty
Q	Inlet (feed) flow rate
Q_n	Normalized inlet flow rate
Q_o	Overflow flow rate
Q_u	Underflow flow rate
Q_{avg}	Mean value of the inlet flow rates
R^2	Coefficient of determination in regression
R_f	Flow ratio; underflow to inlet volumetric flow rate ratio
U_x	Total uncertainty
x	Particle size
PSD	Particle size distribution
RMS	Root mean squared
SE	Standard error of the coefficients in regression
STD	Standard deviation
VIF	Variance inflation factor
α_i	Coefficient in regression, $i = 1,2,\ldots$
β_i	Coefficient in regression, $i = 1,2,\ldots$
ΔP	Overflow pressure drop
ΔP_u	Underflow pressure drop

Since changing the underflow diameter is not always feasible, a valve at the underflow can also be used to control the flow [1], either manually or under automatic control. However, this method runs the risk of blocking the apex [5]. Although solutions to avoid apex blockage have been developed [5], both changing the apex pipe size or using a throttling valve at the underflow have the disadvantage of increased chance of clogging in the underflow pipe. Using a pump can be an alternative method for controlling the underflow flow rate. Since most of the studies in the literature investigate discharging the hydrocyclone outlet to the atmospheric pressure, the lack of information on the influence of controlling the hydrocyclone underflow characteristics is the motivation of this work.

The underflow pumping is comparable with underflow pipe diameter changes in terms of affecting the downstream conditions and controlling the hydrocyclone performance. However, with using a variable frequency drive (VFD) for controlling the underflow pump speed, the underflow pumping can be a robust technique for changing the underflow pressure comparing changing the underflow pipe diameter. This means that the underflow pumping introduced in this research can be used to control the hydrocyclone in an active manner.

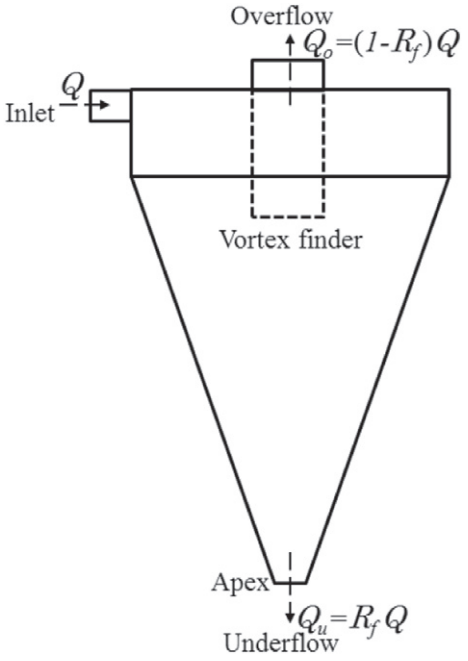

Fig. 1. Schematic of a hydrocyclone and flows.

The use of an underflow pump is examined in this study to understand its influence on the hydrocyclone performance. Typically, the hydrocyclone underflow discharges through the apex to the open at atmospheric pressure. Using a pump in the underflow, the underflow stream can be controlled for varying conditions. In addition, flow blockage in the apex is reduced as the pump promotes flow. In this study the underflow pump is driven by VFD controlled induction motor. Changing the speed of the pump connected to the underflow pipe has a similar effect to changing the underflow discharge orifice diameter [24], but with less chance of clogging.

In the following sections, flow rates, flow ratio, pressures at inlet and outlets and the underflow concentration operating conditions of the hydrocyclone are manipulated variables. Separation performance and grade efficiency are the responding variables, examined for several underflow pumping rates. Pressure ratio $P^* = P_u/P_o$ is here defined as the ratio of absolute underflow pressure P_u to the absolute overflow pressure P_o and is used in this study to evaluate the effect of underflow pumping on the hydrocyclone performance and operating parameters. Unlike a standard hydrocyclone, the experimental system with a variable pump speed allows for significant changes in the underflow pressure.

The ultimate aim of this study is to develop a model for predicting the hydrocyclone performance that have characteristics that can be used for active control. This is undertaken by performing experiments on a hydrocyclone equipped with an underflow pump. Following the experiments, a model is developed using the data obtained from the experiments. The model explains the changes in P^* in terms of hydrocyclone operating variables.

2. Experimental setup

A flow diagram of this experimental setup is shown in Fig. 2. A mixture of liquid water and soda lime solid particles is pumped from the mixing tank as the feed stream to the hydrocyclone inlet. The clean part (fine particles) of the separation moves to the overflow of the hydrocyclone and is returned to the mixing tank. The coarser particles leave the hydrocyclone through the underflow pipe and a

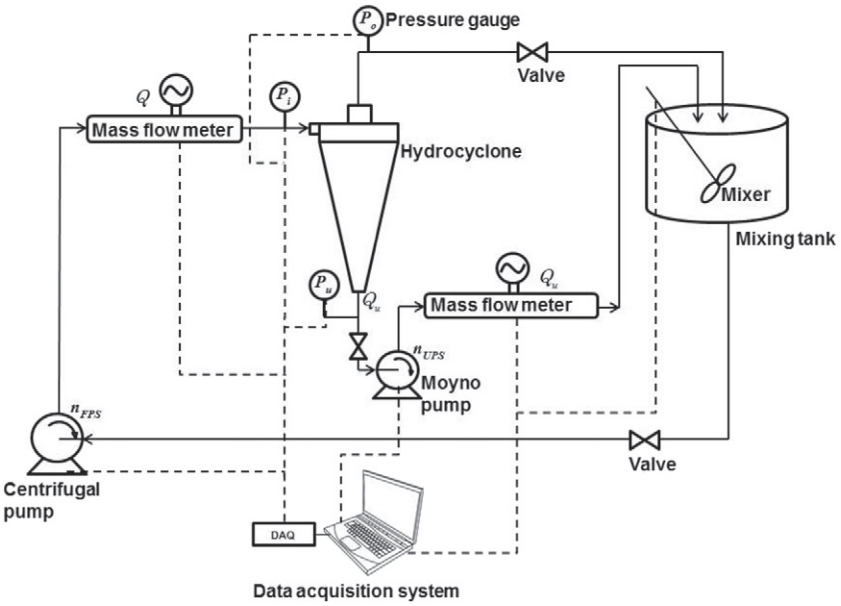

Fig. 2. Schematic of the experimental flow loop.

progressive cavity pump equipped with a VFD. The underflow stream also returns to the mixing tank.

To have a uniform distribution of the particles at the inlet, a mixer is used in the mixing tank. Both the mixer and the pumps (feed and underflow) are equipped with VFDs to control pumping rates. Inlet flow and underflow streams are each measured with a separate Coriolis flow meter (located according to the manufacturers recommendations [25,26]). The mixture and flow properties of flow velocity, flow rate and temperature are measured in each flow meter and transmitted to the data acquisition system. Solids concentration is also determined in the Coriolis flow meter by defining the liquid and solid densities. To minimize the pressure drop effects in the connected pipes on the measurements, pressures in the system are measured near the hydrocyclone inlet and outlets.

Communication lines for flow meter transmitters, VFDs, and pressure gauges that communicate to the data acquisition system are depicted with dashed lines in Fig. 2. Flow samples are taken using sampling ball valves at the hydrocyclone inlet, the overflow, and the underflow pipes. To minimize the sampling errors, the flow stream of the underflow is sampled first, followed by the overflow, and lastly the inlet stream. The samples are used for determining particle size distribution (PSD) with a PSD analyzer using a method described below. A summary of the setup is listed in Table A1 in Appendix A and the hydrocyclone dimensions are detailed in Table 1. A customized control and data log software has also been developed to communicate with the devices and to record the data.

Soda lime glass beads particles with density of 2500 kg/m^3 are mixed with water to obtain nominal solid volume at these three concentrations: 0.1, 0.5 and 2%v/v. The average measured concentrations are 0.111%v/v, 0.480%v/v, and 1.908%v/v, respectively. At each concentration, three different flow rates are established at feed pump speeds of 1200, 1500 and 1800 rpm, while the underflow pump speed is set to six speeds from 300 to 1500 rpm. This results in 54 (3×3×6) test points each of which is run three times to check the repeatability of the experiments. More details on the experimental setup can be found in [27,28].

Table 1
Geometric parameters of the type hydrocyclone.

Geometric portion	Size (mm)
Hydrocyclone diameter, D	50
Inlet pipe hydraulic diameter, D_i	22
Overflow pipe diameter, D_o	12
Cylindrical section length, L_1	62
Vortex finder length[a], l	42
Hydrocyclone total length, L	890

[a] The portion of the overflow pipe that extends into the cyclone.

2.1. Particle size distribution (PSD)

The particle size distribution for each stream sample is obtained using a particle size analyzer detailed in Table A1. Each sample is first diluted as specified by the manufacturer and the accuracy of the size distribution measurements is tested with a known sample. The size distribution measurement is performed for both inlet and outlet streams.

Points of the underflow sample size distribution results are discussed for one specific case. Using a diluted sample from the underflow, the PSD measurement is repeated five times with the repeatability of the measurements. For particle sizes, the confidence interval in measurement is ±1% of the size [29]. It is found that the PSD measurements are repeatable with a maximum standard deviation of 1.23×10^{-2} in the cumulative distribution. For each measurement, the D_{50} the median size is found. D_{50} is the size that has cumulative distribution equal to 0.5 or 50%. The average D_{50} of the particles in the underflow is 6.10 ± 0.102μm at 95% confidence level.

2.2. Uncertainty analysis

Three sets of experiments for each feed flow conditions (feed pump speed n_{FPS}, underflow pump speed n_{UPS} and feed concentration c are used to quantify uncertainty. Both precision (random) uncertainty P_x and bias (systematic) uncertainty B are determined from the experimental data [30]. Combining the two uncertainties using the root sum square formula [30] gives the total uncertainty U_x. For a constant feed pump speed (1800 rpm) and underflow pump speed (1500 rpm) the uncertainty of the main variables and the standard deviation (STD) are listed in Table 2. The average value (mean) of each variable, the minimum uncertainty U_x(min.) and maximum uncertainty U_x(max.) for all 54 experiments are also listed in Table 2. This is used to determine the uncertainty of the pressure ratio in this

Table 2
Standard deviation and uncertainties for the experimental variables at n_{FPS} equal 1800 rpm and n_{UPS} equals 1500 rpm. (Mean, minimum and maximum values are for all 54 experiments).

Variable	STD	P_x	B	U_x	Mean	U_x(min.)	U_x(max.)
Inlet flow rate (m^3/h)	0.014	0.023	0.005	0.023	1.620	0.006	0.044
Underflow flow rate (m^3/h)	0.010	0.016	0.003	0.016	0.755	0.005	0.028
Inlet pressure (kPa)	0.315	0.531	0.004	0.531	88.96	0.303	1.899
Underflow pressure (kPa)	0.456	0.768	0.004	0.768	9.757	0.169	1.031
Overflow pressure (kPa)	0.054	0.091	0.004	0.091	−8.301	0.048	0.261
Inlet stream density (kg/m^3)	0.161	0.272	0.5	0.569	996.3	0.569	2.776
Underflow stream density (kg/m^3)	0.171	0.289	0.5	0.578	998.7	0.289	2.178

study. The uncertainty of the pressure ratio P^* varies between the minimum and maximum values of 0.02 kPa to 0.16 kPa or 2% to 13%.

The uncertainties in the measurements are dependent on several factors such as the uncertainties of the measuring equipment, the conditions at which an experiment is performed, setup conditions and even data analysis. To interpret the changes the uncertainties it is valuable to compare their values as in percent of the mean value for each variable. Further analysis of the data in Table 2 shows that the maximum uncertainty in the experiments is for underflow pressure which is 7.8% that is a reasonable value for the experimental work. The highest uncertainty for the underflow pressure can be due to the effect of changes in flow pattern in the hydrocyclone (particularly aircore formation) that influences the underflow pressure sensor and hence the measurement.

3. Results and discussion

As a baseline, the experiments are initially performed with only water in the system and the results for the changes in flow rates have been previously published [24]. Then experiments with varying concentration of solid particles to liquid are then performed.

3.1. Efficiency

The nature of flow splitting in the hydrocyclone results automatically in some efficiency. The inlet flow splits into two streams and each stream goes to either of the outlets (see Fig. 1). Since each part includes a mixture of solid and liquid particles, this leads to some efficiency regardless of the operating conditions. For this reason, the flow splitting separation efficiency is subtracted from the grade efficiency $G(x)$, where x is particle size, to remove the effect of flow splitting on grade efficiency such that [31]:

$$G'(x) = \frac{G(x) - R_f}{1 - R_f} \tag{1}$$

where $G'(x)$ is the resulting efficiency and is called reduced grade efficiency and R_f is flow ratio that is the ratio of the underflow flow rate to the inlet flow rate. This $G'(x)$ is used to compare the separation efficiencies under different conditions or for different hydrocyclone devices.

The influence of the underflow pumping (n_{UPS}) on the reduced grade efficiency [5] curve ($G'(x)$ at a constant feed pump speed (1800 rpm) is shown in Fig. 3. The cut size associated with this plot is called the reduced cut size (d'_{50}) and is equal to 4.4 μm. The plots of $G'(x)$ show that using the pump in the underflow does not have significant effect on the reduced grade efficiency and it mainly changes the flow ratio. The effect of underflow pumping and flow ratio will be discussed later in Section 3.2.4.

To evaluate the effect of the concentration on the reduced grade efficiency, the curves of $G'(x)$ at a constant feed pump speed (n_{FPS} = 1800 rpm), a constant underflow pump speed (n_{UPS} = 1500 rpm) and for varying concentrations are plotted in Fig. 4. Increasing the concentration from 0.1%v/v to 2%v/v in the feed stream of the hydrocyclone leads to an increase in the separation reduced cut size from 4.88μm to 5.94 μm as shown in Fig. 4. As there is only a small change in feed concentration, the curves are not significantly different; however, they follow the trend that is observed by increasing the inlet concentration [32].

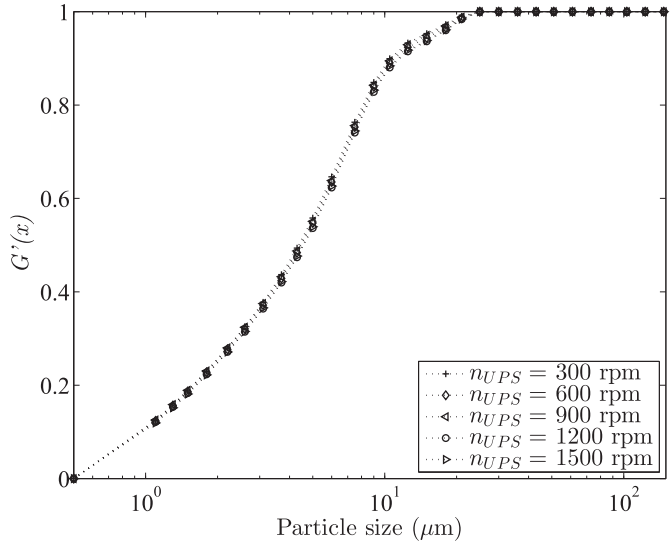

Fig. 3. Effect of underflow pumping on the reduced grade efficiency $G'(x)$ of the hydrocyclone for different underflow pump speeds; n_{FPS} = 1800 rpm; c = 0.5%.

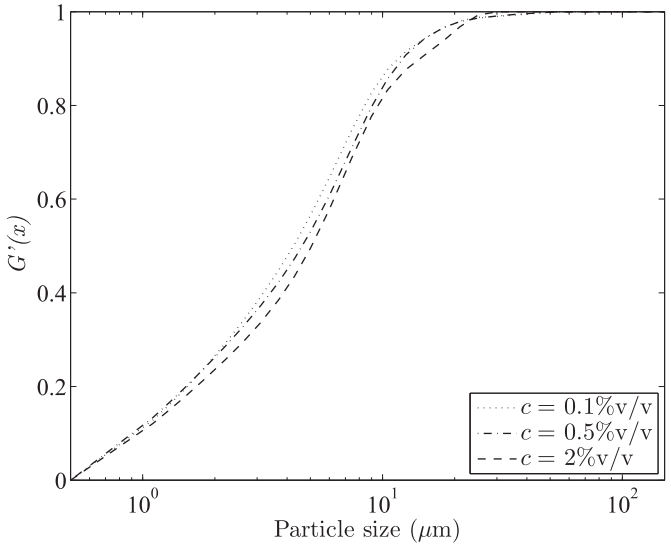

Fig. 4. Effect of concentration on the reduced grade efficiency of hydrocyclone; n_{FPS} = 1800 rpm, n_{UPS} = 1500 rpm.

3.2. The underflow pumping effect on the hydrocyclone operation

The effect of using the underflow pump on flow rate, flow ratio, and pressures is investigated as a function of pressure ratio $P^* = P_u/P_o$. This is a non-dimensional variable that represents the underflow pressure changes. The rationale for this investigation is discussed next.

3.2.1. Inlet flow rate

The effect of the changes in the inlet (feed) flow rate Q with respect to P^* is plotted in Fig. 5 for three feed pump speeds. It shows that the inlet flow rate decreases slightly with increasing the pressure ratio. This is comparable with a trend of changes in the flow rates with respect to the underflow to overflow diameter ratio reported in the literature [5]. Inlet flow rate Q does not change significantly with changes in the underflow to the overflow pipe diameter D_u/D_o ratio [5]. This leads to the idea that P^* can be used to control the hydrocyclone performance in an analogous way to changing the underflow pipe size. The influences of P^* and D_u/D_o are opposing, as increasing P^* has a similar effect on the inlet and the underflow flow rates as that of reducing the underflow/overflow pipe diameter ratio.

3.2.2. Inlet and outlet pressures

Changes in the inlet pressure P_i, overflow pressure P_o, overflow pressure drop $\Delta P = P_i - P_o$, and underflow pressure P_u as a function of pressure ratio P^* are shown in Fig. 6 to Fig. 9 (all pressures are absolute). Increasing the pressure ratio does not have a significant effect on the inlet pressure or the pressure drop, as seen in Fig. 6 and Fig. 8, respectively.

The overflow pressure shown in Fig. 7 increases with the pressure ratio, although the amount is less than 1 kPa (1%) at each n_{FPS}. This increase is not significant when comparing the order of magnitude of the other pressures in the experiment. This is also shown in Fig. 7 for a different scale on the right vertical axis. Since the inlet pressure is not significantly affected by underflow pumping, the upstream pressure is almost independent of the downstream pressure changes. This is similar to changes in the underflow pipe diameter or underflow flow rate by using a valve, showing that underflow pumping can be used to achieve a similar effect. The overflow pressure can also be considered as a constant pressure relative to the inlet and underflow pressures. This means $P^* = P_u/P_o$ is only affected linearly by underflow pressure P_u. Therefore, P^* can be used as a normalized variable that represents the behavior of the underflow pressure.

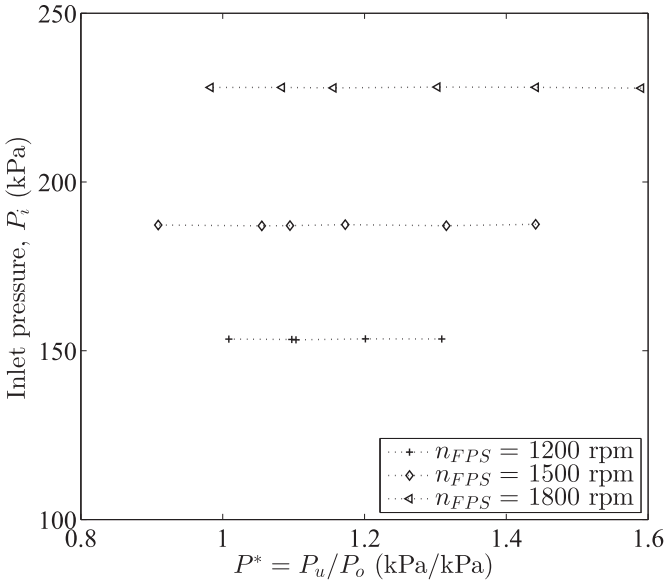

Fig. 6. Inlet pressure: effect of changes in the pressure ratio at three feed pump speeds n_{FPS}; $c = 2\%$v/v.

The linearity of P^* in underflow pressure is seen in Fig. 9. This is to show that the pressure ratio represents the underflow pressure in terms of a dimensionless variable. Increasing the pressure ratio by increasing the underflow pressure means less suction in the underflow pipe. Comparing the pressure changes from Fig. 6 to Fig. 9, the pressure ratio P^* has the strongest (almost linear) effect on the underflow pressure. This response indicates that the underflow pressure drop $\Delta P_u = P_i - P_u$ is the most effective pressure drop in this experimental setup for predicting the hydrocyclone performance.

3.2.3. Underflow concentration

The influence of pressure ratio on the underflow discharge concentration c_u is shown in Fig. 10 for three different feed concentrations. As the underflow pump speed decreases (higher P^* and less suction in the underflow) it is expected that less water is pulled toward the underflow and the underflow concentration increases,

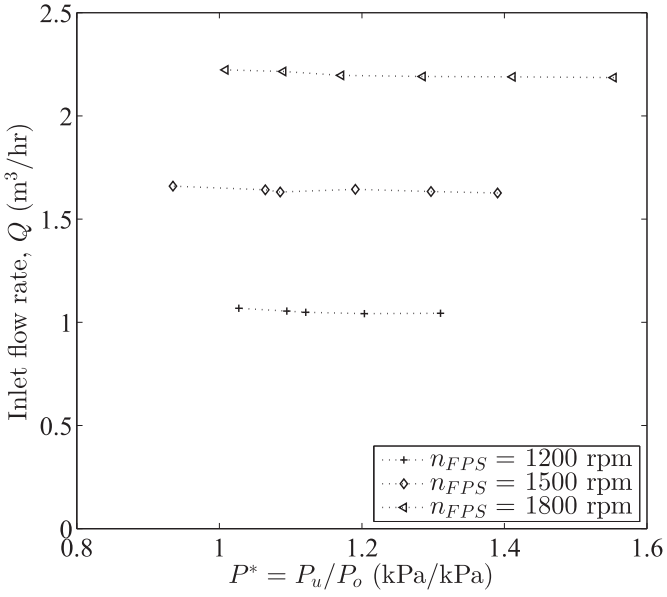

Fig. 5. Inlet flow rate: effect of changes in the pressure ratio at three feed pump speeds (n_{FPS}); $c = 0.5\%$v/v.

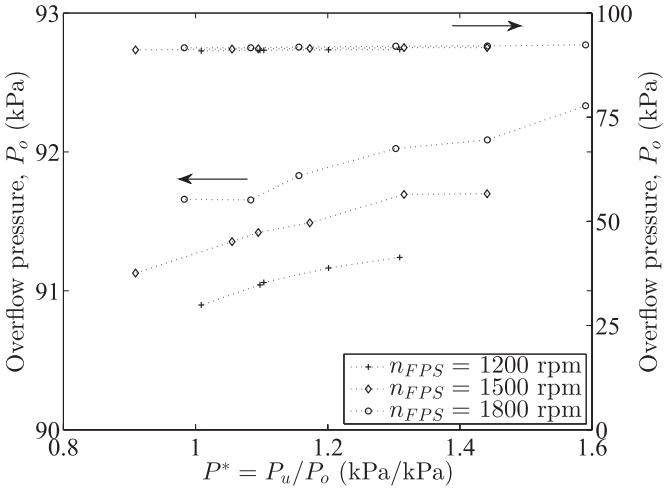

Fig. 7. Overflow pressure: effect of changes in the pressure ratio at three feed pump speeds n_{FPS}; $c = 2\%$v/v.

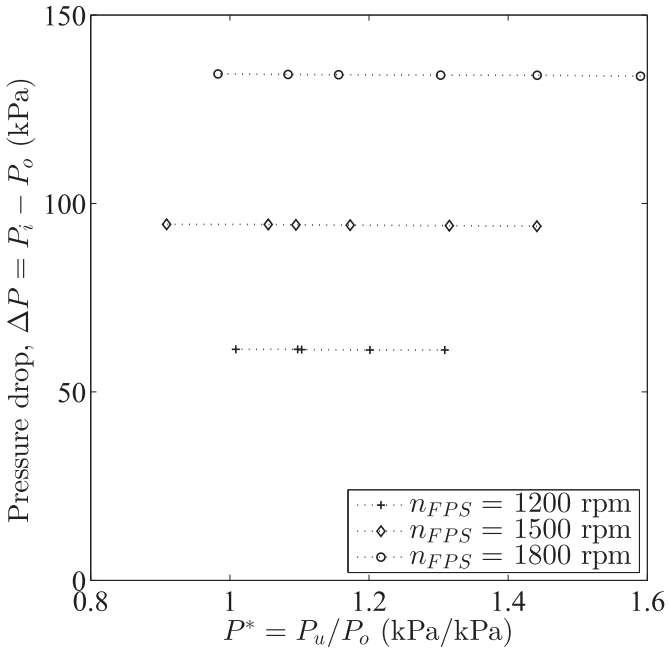

Fig. 8. Pressure drop: effect of changes in the pressure ratio at three feed pump speeds n_{FPS}; $c = 2\%$v/v.

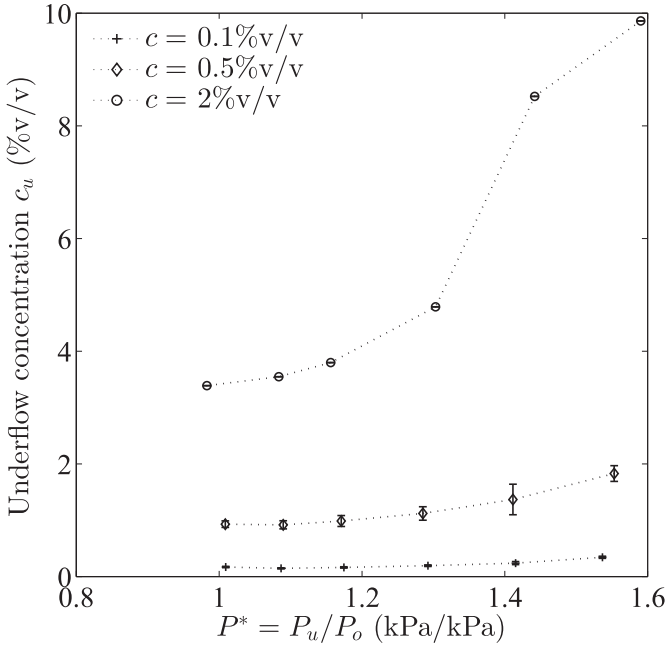

Fig. 10. Effect of changes in the pressure ratio on the underflow solid volume concentration at different feed concentration; $n_{FPS} = 1800$ rpm.

as shown in Fig. 10. Of course, increasing the feed concentration increases the underflow concentration. To evaluate the interaction of feed concentration and the underflow pumping effect, c_u is normalized with the feed the concentration c and the results are plotted in Fig. 11. An increase in the normalized concentration $\bar{c}_u = c_u/c$ when the feed concentration increases from 0.1%v/v to 2%v/v as the pressure ratio increases is shown in Fig. 11. The curves of 0.5%v/v and 2%v/v feed concentration for pressure ratios less than 1.3 are within the experimental uncertainty. The plot of 2%v/v concentration is located within the error bars of the plot of 0.5%v/v concentration. However, an increase in the $\bar{c}_u = c_u/c$ is observed above $P^* = 1.3$.

3.2.4. Flow ratio $R_f = Q_u/Q$

The flow ratio is an important parameter in controlling a hydrocyclone, as this ratio is a direct function of the inlet flow rate Q or the underflow flow rate Q_u. To understand the behavior of the flow ratio with respect to the underflow pumping, the effect of the pressure

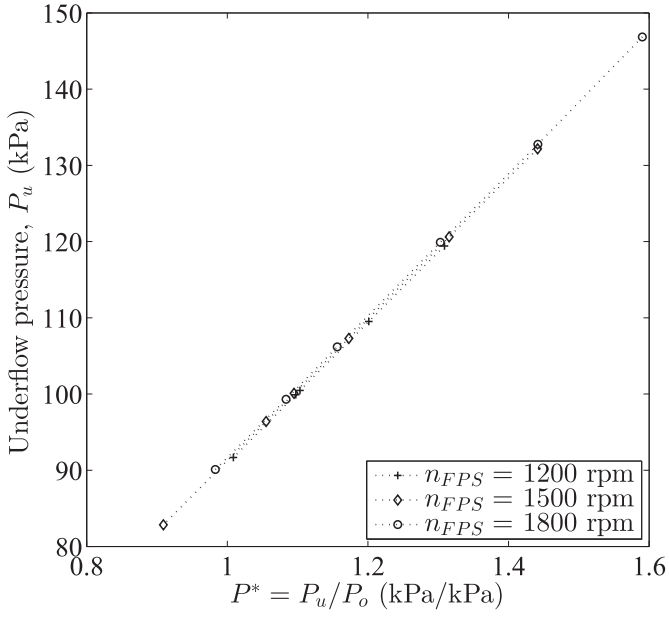

Fig. 9. Underflow pressure: effect of changes in the pressure ratio at three feed pump speeds n_{FPS}; $c = 2\%$v/v.

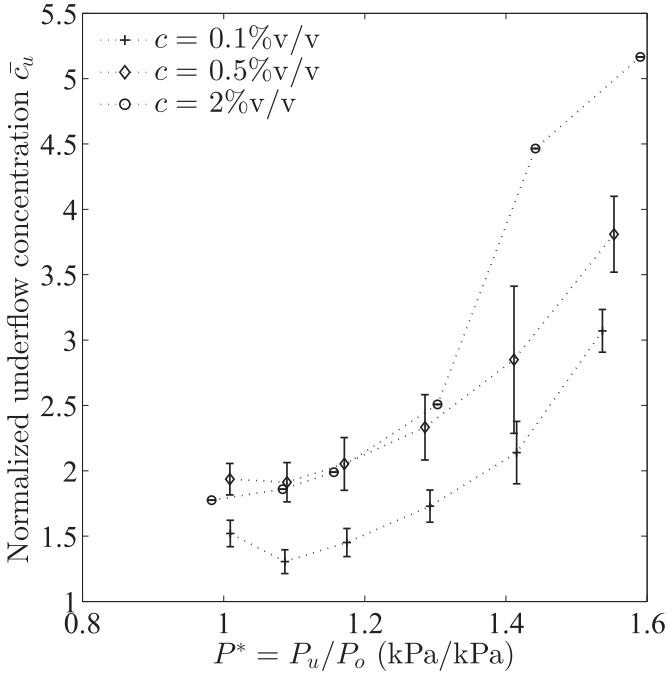

Fig. 11. Effect of changes in the pressure ratio on the normalized underflow solid volume concentration $\bar{c}$ at different feed concentration; $n_{FPS} = 1800$ rpm.

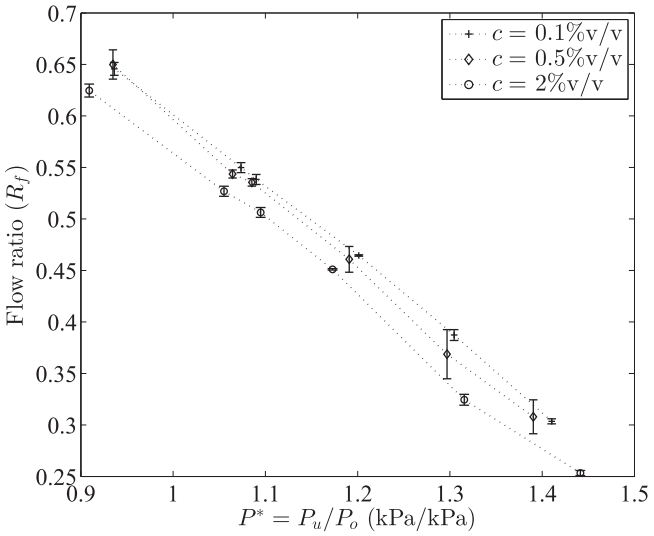

Fig. 12. Effect of changes in the pressure ratio on the flow ratio at different feed concentration; n_{FPS} = 1500 rpm.

ratio P^* on the R_f is shown in Fig. 12. As a result of reduced suction, R_f decreases when increasing the pressure ratio. Increasing the concentration decreases R_f which results in less flow in the underflow (for a fixed inlet flow rate) at higher concentrations. This is expected and is attributed to the accumulation of solids in the underflow discharge zone, which reduces the discharge area and results in a higher flow rate through the overflow pipe. The small reduction in the inlet flow rate with increasing P^*, observed in Fig. 5, is also a factor; but it is not as significant as the changes in the underflow flow rate.

The trend of changes in flow ratio with respect to P^* matches the trends of underflow flow rate with underflow to overflow pipe diameter ratio [5] similar to that discussed for the inlet flow rate changes with pressure ratio. This confirms the previous understanding about using the P^* for controlling the hydrocyclone performance.

3.3. Model development for predicting pressure ratio

The development of a correlation for predicting the effect of the underflow pumping and comparing it to changing underflow/overflow diameter is a major objective of this study. The main performance factors are: pressures and flow rates at the hydrocyclone inlet and outlets, inlet concentration, and inlet particle cut size. Both linear and nonlinear regression approaches are applied to find the model that can best capture the pressure ratio and hence underflow pressure changes for the experimental data set. The fixed parameters in the experiment (such as liquid and solid densities, the density difference, and diameters) are not involved in the model development.

The underflow pumping effect is evaluated using the pressure ratio P^*. Models consisting of pressure drop, inlet cut size, inlet concentration, inlet flow rate, and flow ratio are tested for predicting the pressure ratio. From the initial statistical analysis of the experimental data, the inlet particle cut size is found not to be significant variables. Thus, the predictor parameters involved in the model development are normalized inlet flow rate ($Q_n = Q/Q_{avg}$) where Q_{avg} is the mean value for all recorded flow rates, flow ratio (R_f), normalized pressure drop ($\Delta P/P_i$), and inlet solid volume concentration (c). Predictors are assumed to be independent of each other and the possibility of any correlation between these variables will be obtained using statistical analysis. The non-significant variables or the variables which are correlated are removed from the regression model.

Table 3
Pressure ratio (P^*) linear regression.

Coefficient	Estimate	SE	t-Statistics	p-Value
α_0	1.5630	0.0484	32.301	1.26E−35
α_2	−0.7421	0.0866	−8.5649	1.92E−11
α_4	−0.0037	0.0191	−0.1978	0.8439
RMS error	0.111		R^2	0.59
Model p-value	1.27E−10		Adjusted R^2	0.57

3.3.1. Linear regression approach

For the linear regression, polynomials of different orders up to fourth-order for the function variables are tested. Using statistical hypothesis tests for significance level of the coefficients, a polynomial function of the order of one is found to be more significant than others. The linear model is then in the form:

$$P^* = \alpha_0 + \alpha_1 Q_n + \alpha_2 R_f + \alpha_3 \Delta P/P_i + \alpha_4 c \quad (2)$$

To check if there is any correlation between the predictors, variance inflation factor (VIF) [33] that is an indicator of collinearity is used. Details of the VIF concept and its interpretation can be found in [33]. By computing VIF for the predictors, it is found that the normalized flow rate and pressure drop are not independent variables. This is in agreement with what is expected from the physics of the hydrocyclones for inter-correlation between these factors.

Removing Q_n and $\Delta P/P_i$ from Eq. (2), the statistical information for estimated coefficient for the linear correlation function is presented in Table 3. This is including standard error (SE) of the coefficients that measures how precisely the model estimates the coefficient, root mean squared (RMS) error (which is a measure of the spread of the estimated response values around their average), t-statistics and p-value (an indication of significance of estimated coefficient or model under investigation for regression analysis), R^2 (an indication of the goodness of a fit) and adjusted R^2 (adjusted R^2 for the number of parameters involved in the regression) [34].

Typically coefficients with p-values smaller than 0.05 are considered to be significant [35]. As can be seen from Table 3, this value for the inlet concentration coefficient (α_4) is noticeably greater than 0.05. This means that the linear regression model predicts that the flow ratio is the variable that causes significant changes in pressure ratio. Considering the goodness of the fit R^2, the closer the value of R^2 to 1, the better fit is expected. This value is 0.59 in this linear regression. It is also found that removing the concentration variable from the regression does not improve this number. Nonlinear regression analysis is applied to the data of the experiment to obtain a better fit.

3.3.2. Nonlinear regression approach

To obtain a model with a better goodness-of-fit R^2, nonlinear modeling is also performed. Similar to linear regression, R_f and c are used to be the main parameters involved in predicting P^*. Using trial and error with some nonlinear functions, a useful predicting function is found to be:

$$P^* = R_f^{\beta_1} \exp(\beta_2 c) \quad (3)$$

Table 4
Pressure ratio (P^*) nonlinear regression.

Coefficient	Estimate	SE	t-Statistics	p-Value
β_1	−0.2689	0.0153	−17.604	1.4698E−23
β_2	−0.0267	0.0122	−2.1941	0.0327
RMS error	0.0892		R^2	0.721
Model p-value	9.49E−60		Adjusted R^2	0.716

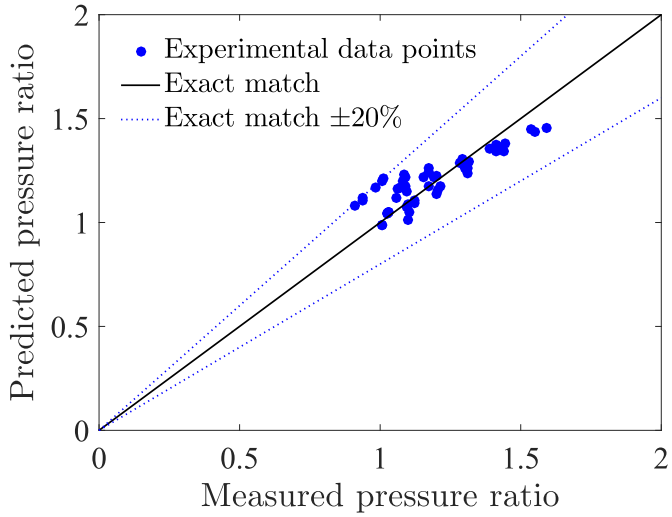

Fig. 13. Pressure ratio nonlinear regression: a comparison of measured and predicted values of pressure drop ratio P^*.

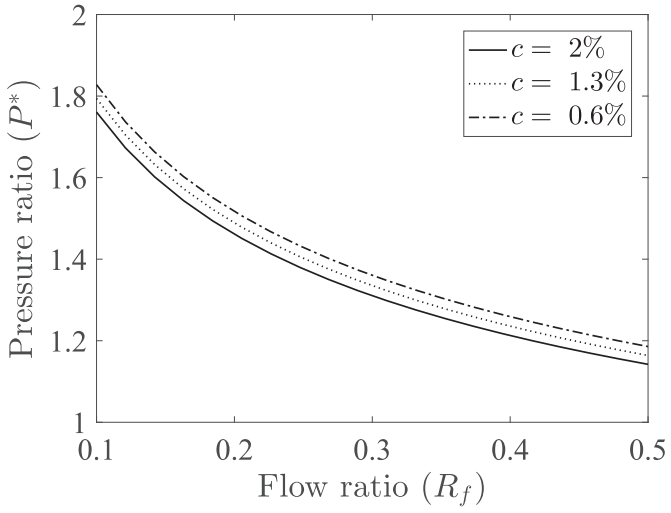

Fig. 15. Effect of changes in flow ratio on pressure ratio.

The statistics related to the nonlinear regression are listed in Table 4. Both coefficients of the nonlinear model in Eq. (3) are found to be significant as the p-values are smaller than 0.05. Unlike the linear regression modeling, solids concentration is observed to have more significant role in predicting the pressure ratio in this nonlinear model. A comparison of the model to the experimental is plotted in Fig. 13 and shows that the nonlinear model predicts the pressure ratio within ±20% deviation from the experimental results.

3.3.3. Model selection

Investigating the statistics of the both linear and nonlinear models presented in Eqs. (2) and (3), and Table 3 and Table 4, it is clear that the nonlinear model provides a more accurate prediction of the experimental data. The correlation, to predict the pressure ratio for the hydrocyclone design, is valid for a solids volume concentration lower than 2%v/v and is based on the experimental data is:

$$P^* = R_f^{-0.2689} \exp(-0.0267c) \tag{4}$$

This correlation is unit-less and can be used with any system of units.

To validate the model, a separate test with the experimental setup is performed at a different concentration (c = 1%) and the data is used to validate the model. This separate test is undertaken since no similar setup (with a pump in the underflow) is seen in the literature. The results of this cross validation are shown in Fig. 14. The nonlinear model predicts the pressure ratio within ±15% from the experimentally observed values for this new test.

The coefficients of Eq. (4) indicate that the flow ratio has a stronger effect on pressure ratio than feed concentration. The effect of changes in the pressure ratio with flow ratio at three different solid concentration is shown in Fig. 15. It can be seen that as pressure ratio decreases the flow ratio increases, showing increase in the underflow flow rate.

The slopes of changes in P^* with respect to changes in each model variables are plotted versus flow ratio R_f in Figs. 16 and 17 for three nominal solid volume concentration. The changes in P^* with respect to R_f is two orders of magnitude greater than changes

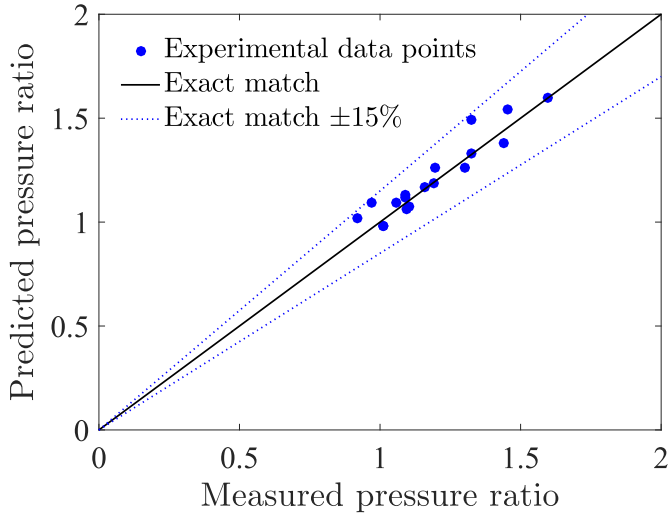

Fig. 14. Cross validation for pressure ratio using nonlinear developed model; c = 1%v/v.

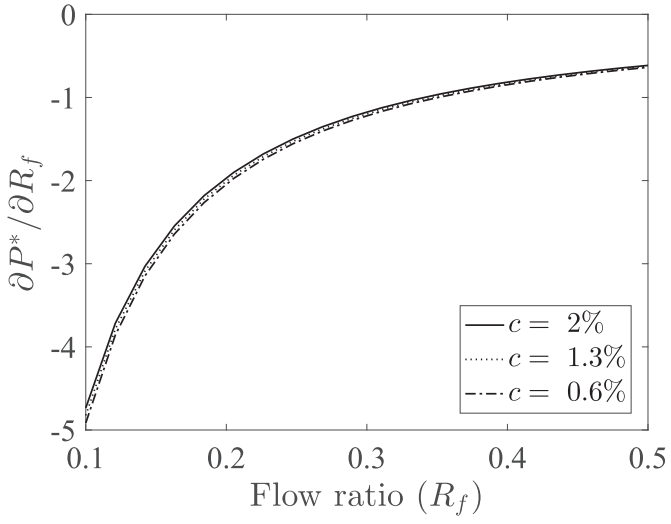

Fig. 16. Pressure ratio sensitivity to flow ratio.

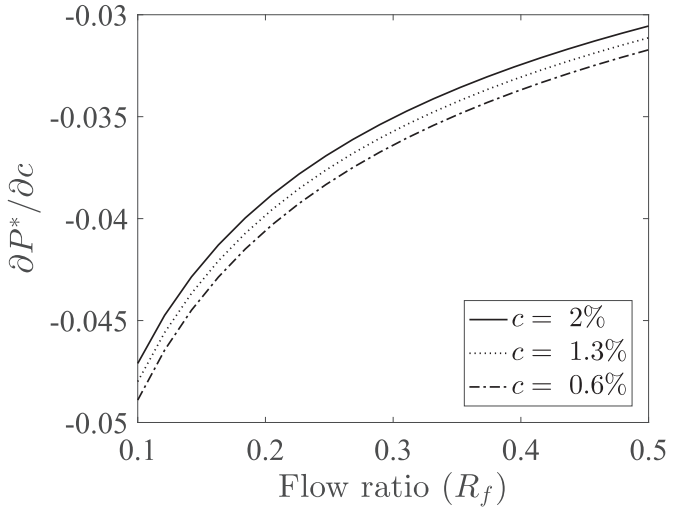

Fig. 17. Pressure ratio sensitivity to inlet volume concentration.

with respect to c. This shows that the pressure ratio P^* is most sensitive to the flow ratio, and that the inlet solid volume concentration has less influence on P^*. Therefore, the flow ratio is the most effective way to manipulate the pressure ratio for controlling the hydrocyclone performance at low inlet solid concentration. This correlation can be used for further study on hydrocyclone control.

The model developed in this research is subject to limits of the experiments undertaken which includes the effect of the inlet flow conditions. The effect of inlet solid volume fraction is limited to a maximum fraction of 2%. The model cannot be used to interpret the influence of hydrocyclone design parameters such as inlet and outlet diameters as these are not included in the model. The developed correlation is based on a certain hydrocyclone size to highlight the effects of variables using an underflow pump. Further experiments are needed to generalize the model for different hydrocyclone sizes and variety of design parameters and inlet flow conditions.

4. Conclusions

The effect of hydrocyclone underflow pumping is studied experimentally by using the soda lime particles in water. Three different solid concentrations (maximum 2%v/v) are examined at different flow rates by changing the feed pump speed.

The results of the study show that increasing the feed volume solid concentration from 0.1% to 2% increases the separation reduced cut size from 4.88 μm to 5.94 μm. The ratio of the underflow to overflow absolute pressures is defined as pressure ratio P^* and is used to study the underflow pumping effect on the performance. The changes in the inlet flow rate and underflow rate with the pressure ratio shows that the inlet flow rate increases slightly with decreasing pressure ratio and the underflow flow rate increases significantly with decreasing the pressure ratio. These trends are similar to increasing the underflow pipe diameter, which is another method of adjusting the hydrocyclone performance according to the feed flow conditions. The changes in the inlet and outlet pressures and overflow pressure drop are also studied; but no significant changes are observed with the underflow pumping.

The data of the 54 experimental trials are used to develop a correlation to predict the pressure ratio. Equations found by linear and nonlinear regression show that the nonlinear model provides a better fit with predicting the hydrocyclone behavior. A nonlinear model, for predicting the pressure ratio within the limits of this study, is defined (Eq. (4)). It is observed that the most and least sensitive influencing variables on the pressure ratio are flow ratio and inlet concentration, respectively. Using a pump in the underflow of a hydrocyclone separator can help adjust the device to accommodate fluctuations in the inlet flow. This is similar to using a valve in the underflow or changing the apex size; and the underflow pump is used to control the hydrocyclone performance. This model can be used for further studies on controlling the hydrocyclone separation performance.

Acknowledgments

Financial support from the Natural Sciences and Engineering Research Council of Canada (NSERC) and the Canada Foundation for Innovation (CFI) is gratefully acknowledged.

Appendix A. Details of equipment and data acquisition system

Table A1
Experiment equipment summary.

Device	Model	Maker	Specifications
Centrifugal pump	XR-2(7)	Hayward Gordon Inc., Canada	1780 rpm, 40 ft head, 143 USgpm
VFD	ESV552N02TXB	Lenze, USA	4–20 mA w/500 ohm total impedance
Electric motor		Weg	5.5 kW
Progressive cavity pump	33204 mechanical seal	Moyno, Inc., USA	0–100 psi discharge pressure
VFD	ID15H201-E	Baldor, USA	AC INVERTER, 230 V, serial communication
Electric motor		Baldor Electric, USA	0.37 kW, 1750 rpm, 6000 max. rpm
Pressure gauge	AST4000	American Sensor Technologies (AST), USA	4–20 mA, accuracy is 0.4% BFSL, 0 to 200 kPa
Coriolis flow meter	Promass 83I	Endress + Hauser Ltd, Canada	±0.05% maximum error, 4 to 20 mA
Coriolis flow meter	Optimass7300	Krohne Messtechnik GmbH, Germany	±0.1% of actual flow ± 0.0018 m^3/h maximum error, MFC300 transmitter, Modbus over RS485, 32 per line
Mixer	PHG Gear Drive	Promix	Hydrofoil impeller
VFD	174610.00	Leeson Electric, USA	1.5 kW, 7 A, 3 ph
Electric motor	C6T17FB65F	Leeson Electric, USA	1.49 kW
PSD analyzer	HELOS/BR	Sympatec GmbH, Germany	_x0006_1% deviation with respect to the standard meter, measuring range from 0.1 m to 8750 m
Hydrocyclone	U2-GMAX-3020	FLSmidth Krebs, USA	Krebs cyclone, 4–50 psi, G85LG-45-RU Apex, 4–50 psi, dimensions are listed in Table 1

References

[1] D. Bradley, The Hydrocyclone, Pergamon Press Ltd., Oxford, London, 1965.
[2] M. Habibian, M. Pazouki, H. Ghanaie, K. Abbaspour-Sani, Application of hydrocyclone for removal of yeasts from alcohol fermentations broth, Chem. Eng. J. 138 (1–3) (2008) 30–34. http://dx.doi.org/10.1016/j.cej.2007.05.025.
[3] T. Neesse, H. Tiefel, P. Kaniut, Volume split control of a hydrocyclone group, Miner. Eng. 20 (4) (2007) 355–360. http://dx.doi.org/10.1016/j.mineng.2006.12.004.
[4] R.K. Tue Nenu, Y. Hayase, H. Yoshida, T. Yamamoto, Influence of inlet flow rate, pH, and beads mill operating condition on separation performance of submicron particles by electrical hydrocyclone, Adv. Powder Technol. 21 (3) (2010) 246–255. http://dx.doi.org/10.1016/j.apt.2009.11.010.
[5] L. Svarovsky, Hydrocyclones, Holt Rinehart and Winston. 1984.
[6] M.H. Shojaeefard, A.R. Noorpoor, H. Yarjiabadi, M. Habibian, Particle Size Effects on Hydro-cyclone Performance, 17 (3) (2006) 9–19.
[7] B.A. Wills, T. Napier-Munn, Wills' Mineral Processing Technology, 7th ed., Elsevier Science & Technology Books. 2005. http://dx.doi.org/10.1016/B978-075064450-1/50000-X.
[8] Y. Zhang, P. Qian, Y. Liu, H. Wang, Experimental study of hydrocyclone flow field with different feed concentration, Ind. Eng. Chem. Res. 50 (13) (2011) 8176–8184. http://dx.doi.org/10.1021/ie100210c.
[9] T. Dyakowski, L.F.C. Jeanmeure, A.J. Jaworski, Applications of electrical tomography for gas-solids and liquid-solids flows - a review, Powder Technol. 112 (3) (2000) 174–192. http://dx.doi.org/10.1016/S0032-5910(00)00292-8.
[10] V. Krishna, R. Sripriya, V. Kumar, S. Chakraborty, B. Meikap, Identification and prediction of air core diameter in a hydrocyclone by a novel online sensor based on digital signal processing technique, Chem. Eng. Process. Process Intensif. 49 (2) (2010) 165–176. http://dx.doi.org/10.1016/j.cep.2010.01.003.
[11] L. Chu, W. Chen, X. Lee, Enhancement of hydrocyclone performance by controlling the inside turbulence structure, Chem. Eng. Sci. 57 (1) (2002) 207–212. http://dx.doi.org/10.1016/S0009-2509(01)00364-5.
[12] H. Schlaberg, F. Podd, B. Hoyle, Ultrasound process tomography system for hydrocyclones, Ultrasonics 38 (1–8) (2000) 813–816.
[13] R. Hou, A. Hunt, R. Williams, Acoustic monitoring of hydrocyclones, Powder Technol. 124 (3) (2002) 176–187. http://dx.doi.org/10.1016/S0032-5910(02)00025-6.
[14] J.V.V. Magrieta Jeanette, A. Chris, A. Lidia, B. Chandon, D.J. Corné, On-line monitoring of dynamic hydrocyclone behaviour, Automation in Mining, Mineral and Metal Processing, 13th IFAC Symposium on Automation in Mining, Mineral and Metal Processing, University of Stellenbosch, South Africa. 2010, pp. 87–91. http://dx.doi.org/10.3182/20100802-3-ZA-2014.00021.
[15] T. Neesse, M. Schneider, J. Dueck, V. Golyk, S. Buntenbach, H. Tiefel, Hydrocyclone operation at the transition point rope/spray discharge, Miner. Eng. 17 (5) (2004) 733–737. http://dx.doi.org/10.1016/j.mineng.2004.01.014.
[16] Z. Liu, Y. Zheng, L. Jia, Q. Zhang, An experimental method of examining three-dimensional swirling flows in gas cyclones by 2D-PIV, Chem. Eng. J. 133 (2007) 247–256. http://dx.doi.org/10.1016/j.cej.2007.02.015.
[17] M. Schneider, T. Neess e, Overflow-control system for a hydrocyclone battery, Int. J. Miner. Process. 74 (2004) S339–S343. http://dx.doi.org/10.1016/j.minpro.2004.07.037.
[18] I.C. Bicalho, J.L. Mognon, J. Shimoyama, C.H. Ataíde, C.R. Duarte, Effects of operating variables on the yeast separation process in a hydrocyclone, Sep. Sci. Technol. 48 (6) (2013) 915–922. http://dx.doi.org/10.1080/01496395.2012.712597.
[19] J. Dueck, E. Pikushchak, L. Minkov, M. Farghaly, T. Neesse, Mechanism of hydrocyclone separation with water injection, Miner. Eng. 23 (4) (2010) 289–294. http://dx.doi.org/10.1016/j.mineng.2010.01.002.
[20] K.U. Bhaskar, B. Govindarajan, J.P. Barnwal, K.K. Rao, T.C. Rao, Modelling studies on a 100 mm water-injection cyclone, Physical Separation in Science and Engineering 13 (3–4) (2004) 89–99. http://dx.doi.org/10.1080/14786470412331286580.
[21] R.K. Tue Nenu, H. Yoshida, K. Fukui, T. Yamamoto, Separation performance of sub-micron silica particles by electrical hydrocyclone, Powder Technol. 196 (2) (2009) 147–155. http://dx.doi.org/10.1016/j.powtec.2009.07.011.
[22] A.A. Ahmed, G.A. Ibraheim, M.A. Doheim, The influence of apex diameter on the pattern of solid/liquid ratio distribution within a hydrocyclone, J. Chem. Technol. Biotechnol. 35A (1985) 395–402. http://dx.doi.org/10.1002/jctb.5040350803.
[23] K. Saengchan, A. Nopharatana, W. Songkasiri, Enhancement of tapioca starch separation with a hydrocyclone: effects of apex diameter, feed concentration, and pressure drop on tapioca starch separation with a hydrocyclone, Chem. Eng. Process. Process Intensif. 48 (1) (2009) 195–202. http://dx.doi.org/10.1016/j.cep.2008.03.014.
[24] R. Sabbagh, M.G. Lipsett, C.R. Koch, D.S. Nobes, Theoretical and experimental study of hydrocyclone performance and equivalent settling area, Proceedings of the ASME 2014 International Congress & Exposition IMECE2014, ASME, Montreal, Canada, 2014, http://dx.doi.org/10.1115/IMECE2014-37482.
[25] Optimass 7000 technical datasheet, 2009. (TD OPTIMASS 7000 R08 en), Krohne Messtechnik GmbH & Co. KG, Duisburg
[26] Proline Promass 80I, 83I Technical Information (TI075D/06/en/05.10), Endress + Hauser, Reinach, 2010.
[27] R. Sabbagh, Theoretical and Experimental Investigation of Hydrocyclone Performance and the Influence of Underflow Pumping Effect, University of Alberta, Edmonton, 2015, Ph.D. thesis.
[28] R. Sabbagh, M.G. Lipsett, C.R. Koch, D.S. Nobes, Predicting equivalent settling area factor in hydrocyclones; a method for determining tangential velocity profile, Sep. Purif. Technol. 163 (2016) 341–351. http://dx.doi.org/10.1016/j.seppur.2016.03.009.
[29] W. Witt, T. Stübinger, J. List, Laser diffraction for particle size analysis at absolute precision, World Congress on Particle Technology, WCPT6 2010, Nürnberg, Germany, 2010, pp. 1–4.
[30] A.J. Wheeler, A.R. Ganji, Introduction to Engineering Experimentation, third ed., Prentice Hall, Englewood Cliffs, N.J, 2010.
[31] L. Svarovsky, Solid/liquid Separation, fourth ed., 34. Butterworth-Heinemann. 2000.
[32] T. Braun, M. Bohnet, Influence of feed solids concentration on the performance of hydrocyclones, Chem. Eng. Technol. 13 (1990) 15–20.
[33] L.S.F. Barbara, G. Tabachnick, Using Multivariate Statistics, 6th edition ed., Pearson. 2012.
[34] S. Chatterjee, J.S. Simonoff, Handbook of Regression Analysis, John Wiley & Sons, Inc., Hoboken, New Jersey, 2013.
[35] A. Gelman, J. Hill, Data Analysis Using Regression and Multilevel/hierarchical Models, Cambridge University Press, Cambridge, UK, 2007. http://dx.doi.org/10.2277/0521867061.